INTERNATIONAL JOURNAL FOR NUMERICAL METHODS IN FLUIDS
Int. J. Numer. Meth. Fluids 2000; **32**: 959–977

An improved second moment method for solution of pure advection problems

Abdolreza Ghods, Farhad Sobouti and Jafar Arkani-Hamed*,[1]

Earth and Planetary Sciences, McGill University, 3450 University, Montreal, Quebec Canada H3A 2A7

SUMMARY

The second moment numerical method (SMM) of Egan and Mahoney [Numerical modeling of advection and diffusion of urban area source pollutant. *Journal of Applied Meteorology* 1972; **11**: 312–322] is adapted to solve for the pure advection transport equation in a variety of flow fields. SMM eliminates numerical diffusion by employing a procedure that takes into account the first and second moments of mass distribution in each grid element. For pure translational flow fields, the method is conservative, positive definite and shape-preserving. In rotational and/or shear flows, the accuracy of SMM is significantly reduced. Two improvements are presented to make the SMM applicable to a wider range of flow problems. It is shown that the improved SMM (ISMM) is less diffusive and more shape-preserving than the SMM in rotational and/or deformational flows. The ISMM can also be used to solve for a color function in compressible flow fields. The computational efficiency of this method is compared with that of other methods and, for a given accuracy, it is shown that ISMM is a cost-effective, non-diffusive and shape-preserving method. Copyright © 2000 John Wiley & Sons, Ltd.

KEY WORDS: numerical diffusion; numerical methods; pure advection equation; quasi-Lagrangian method; second moment method; shape preserving

1. INTRODUCTION

The pure advection transport equation is frequently encountered in modeling the compositionally heterogeneous fluid flows associated with geophysical, meteorological and reservoir engineering problems. The presence of sharp material interfaces in such flows requires accurate numerical techniques to prevent numerical diffusion and dispersion. Numerical methods based on Eulerian description usually suffer from numerical diffusion [2] due to truncation errors in the approximation of the spatial derivatives. Lagrangian based methods are accurate but computationally expensive [3], and the interpolative semi-Lagrangian methods are not strictly conservative [4]. One way to reduce the effect of numerical diffusion in a fixed grid is to advect

* Correspondence to: Earth and Planetary Sciences, McGill University, 3450 University, Montreal, Quebec, Canada H3A 2A7.
[1] E-mail: jafar@maho.eps.mcgill.ca

Received 18 May 1998
Revised 6 May 1999

the material in the direction of the velocity field at each time step. The material accumulated in each control volume is then calculated and a mean concentration value is assigned to each grid node. In this sense, the procedure can be regarded as quasi-Lagrangian. One such quasi-Lagrangian method is the second moment method (SMM) of Egan and Mahoney [1], which minimizes numerical diffusion by redistributing the material inside a control volume without introducing unphysical oscillations to the solution. SMM is an explicit forward-in-time method, valid for Courant numbers as high as 1. It is more difficult to implement and it requires considerable memory compared with the Eulerian based methods. SMM was developed to solve the incompressible advective–diffusive transport equation and has been successfully used in atmospheric pollutant transfer [5] and pollutant transfer in surface waterways [6]. It is a shape-preserving, conservative and relatively cost-effective method for purely translational flow fields. These advantages are not entirely shared by other methods. However, its performance is seriously degraded in the rotational and deformational flow fields and it accumulates mass at the stagnation points. In this paper we improve the advection term in SMM and make it useful for solving the pure advection transport equation for a wide range of fluid flows. Our motivation for the improvement emerged from the good performance of the SMM in the transport of pollutants. We essentially make two changes to SMM. The first enhances the accuracy of SMM by reducing the false diffusion associated with non-translational flow fields. The second makes the method capable of handling flow fields with symmetry lines and stagnation points. Furthermore, the improved SMM (ISMM) is useful for advection of a color function in compressible flow fields.

2. BACKGROUND

The equation governing the advection of a tracer field C is

$$\frac{\partial C}{\partial t} + \vec{V} \cdot \nabla C = 0 \tag{1}$$

where $\vec{V}$ denotes the velocity and t is time. The tracer field C specifies the identity of the material. For example, consider a solid body moving inside a fluid. One may designate the solidity as the tracer field. Accordingly, the function C has a value of 1 for the solid and 0 for the fluid. Note that the solidity does not change even if the solid body compacts or expands, although the volume occupied by the body decreases or increases. Another example of a tracer field is the color of a body. A black body remains black even if it is compacted or expanded, implying that the concentration of the tracer does not change even if its volume changes. With this definition of C, it is clear that Equation (1) does not, in general, represent a conservation law, although it becomes one when the medium is incompressible. Therefore, C can specify any scalar variable, such as density, concentration or temperature, in incompressible fluids.

Most conventional backward-time and forward-space difference techniques result in false diffusion in solving Equation (1) [1]. This is because at each time step the material to be advected is assumed to be uniformly distributed over the entire control volume, whereas in the actual advective flow the material may occupy only a fraction of the control volume and does

not overlap the material originally present in the downstream control volumes. SMM suppresses false diffusion by adjusting the material distribution in a control volume at each time step. The tracer field C is represented by a number of discrete rectangular boxes, one box in each control volume. During a time step, the boxes move as rigid bodies within and across the control volumes with the respective nodal velocities in a Lagrangian sense, and are partitioned appropriately between the control volumes (Figure 1). At the end of the time step, the resulting partitioned boxes in a given control volume are combined into a single rectangular box. The x and y co-ordinates of the center of mass of the box (F_x, F_y) are calculated by conserving the first moment of the partitioned boxes with respect to the node of the control volume. The dimensions of the box (R_x, R_y) are determined through conserving the second moment of the partitioned boxes with respect to the center of mass. The mean concentration of the tracer distribution inside the control volume, C_m, the center of mass and the dimensions of the combined box are determined by

$$C_m = \int_{-0.5}^{0.5} \int_{-0.5}^{0.5} C(x, y)\, dx\, dy \tag{2}$$

$$F_x = \frac{1}{C_m} \int_{-0.5}^{0.5} \int_{-0.5}^{0.5} xC(x, y)\, dx\, dy \tag{3}$$

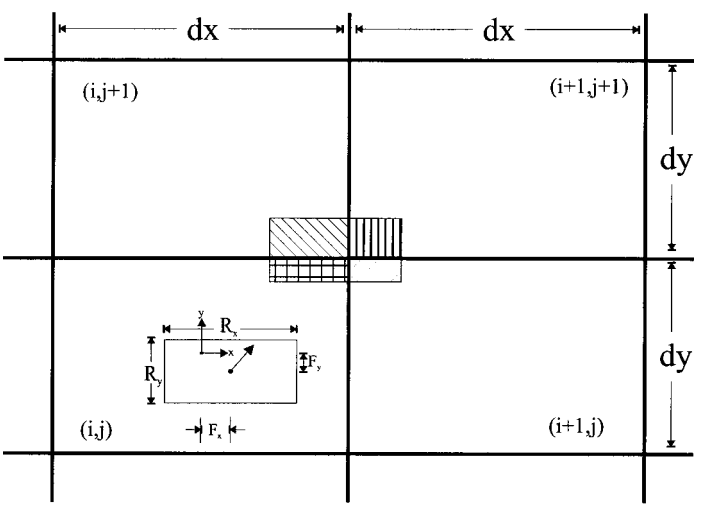

Figure 1. Representation of the tracer field inside a control volume as a rectangular (blank rectangle) box. The solid circle denotes the center of mass of the tracer box. The arrow denotes the velocity vector of the tracer box. During a given time step, the box is advected downstream and appropriately partitioned between the downstream control volumes (the patterned boxes).

$$F_y = \frac{1}{C_m} \int_{-0.5}^{0.5} \int_{-0.5}^{0.5} yC(x, y)\, dx\, dy \tag{4}$$

$$R_x^2 = \frac{1}{C_m} \int_{-0.5}^{0.5} \int_{-0.5}^{0.5} (x - F_x)^2 C(x, y)\, dx\, dy \tag{5}$$

$$R_y^2 = \frac{1}{C_m} \int_{-0.5}^{0.5} \int_{-0.5}^{0.5} (y - F_y)^2 C(x, y)\, dx\, dy \tag{6}$$

where x and y denote the distance of the material from the center of the control volume, and all dimensions are normalized by the dimension of the control volume. They range from -0.5 to 0.5 in both the x- and the y-direction.

As noted by Egan and Mahoney [1] an improvement can be made when the velocity field is curved. The simplest way to find the displacement field $\boldsymbol{\alpha}$ for a given time step Δt is to compute it explicitly from the nodal velocities. However, this does not result in an accurate trajectory path. An alternative procedure is to approximate the trajectory path by first extrapolating the nodal velocity to $t + \frac{1}{2}\Delta t$, and then solving for $\boldsymbol{\alpha}$ iteratively [7]

$$\boldsymbol{\alpha} = \vec{V}\left(\boldsymbol{x} + \frac{1}{2}\boldsymbol{\alpha},\ t + \frac{1}{2}\Delta t\right)\Delta t \tag{7}$$

where $\boldsymbol{x}$ is the position vector. Usually two or three iterations are sufficient to reach a converged solution. A bilinear interpolation is accurate enough to calculate $\vec{V}(\boldsymbol{x} + \frac{1}{2}\boldsymbol{\alpha},\ t + \frac{1}{2}\Delta t)$ [7]. The examples considered in this paper have analytical velocity fields and $\vec{V}(\boldsymbol{x} + \frac{1}{2}\boldsymbol{\alpha},\ t + \frac{1}{2}\Delta t)$ is calculated analytically.

SMM is a positive definite conservative method, and in pure translational flows is diffusion-free and shape-preserving [6]. However, in rotational and deformational flows, the shape-preserving property of the method deteriorates and a significant false diffusion occurs [8,9]. Moreover, a significant amount of mass can be accumulated at the stagnation points. Our improved technique, called hereafter the ISMM, not only alleviates these shortcomings and enhances the performance of SMM, but also enables us to investigate the advection of a tracer field in compressible flows.

3. TREATMENT OF FALSE DIFFUSION

SMM does not preserve the tracer volume in rotational and\or shear solenoidal velocity fields. Any artificial increase (decrease) in the tracer volume results in a decrease (increase) of the concentration of the tracer in a control volume, and hence numerical diffusion (enhancement). To illustrate this point, we consider a control volume initially containing two rectangular distributions, A and B (Figure 2), and calculate R_x and R_y of the rectangular box that is to be combined. In Figure 2(a), the y co-ordinates of the centers of A and B are the same but their x co-ordinates differ. The volume of the combined box calculated from Equations (2)–(6) is equal to the sum of the volumes of boxes A and B. Therefore, the volume is conserved and no

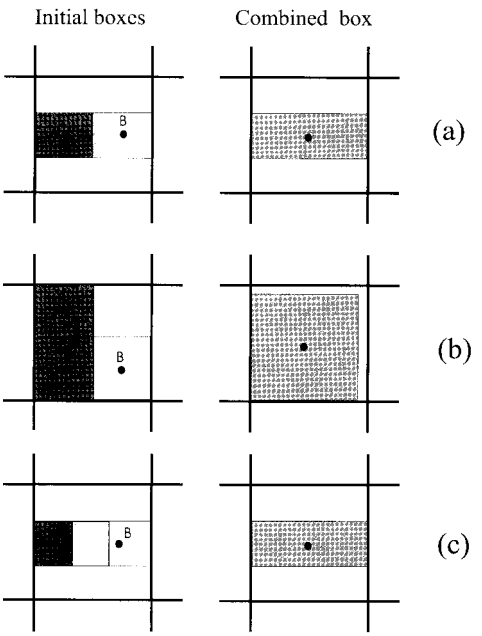

Figure 2. Three possible configurations for two tracer boxes inside a given control volume. The left column shows the constituent boxes A and B, and the right column shows the combined box. The solid circles indicate the centers of mass of the tracer boxes. In (a) the volume of the combined box is equal to the sum of volumes of boxes A and B. In (b) the volume of the combined box is larger than the sum of volumes of A and B and in (c) it is smaller. The hachured area indicates the overlapped part of the two boxes.

numerical diffusion occurs in this case. In Figure 2(b), the co-ordinates of the centers of A and B are different as well as their y dimensions. The mass of tracer inside A and B are 0.5 and 0.25 unit mass respectively (the mass of the tracer box is 1 when it fills the entire control volume). The volume of the combined box calculated by the SMM is about 16.5% larger than the volumes of A and B combined. This results in false diffusion. In Figure 2(c), A and B overlap and SMM results in a volume for the combined box that is smaller than the volumes of A and B by an amount equal to the overlap area. This leads to a false enhancement of the tracer field. Overlapping of the boxes occurs in rotational and shear flow fields due to the fact that SMM neglects cross derivatives of the velocity vector and does not allow the box to rotate or undergo shear deformation.

Realizing the cause of the false diffusion and enhancement, we adjust the dimensions of the combined box to preserve the total volume of the initial partitioned boxes (V_b) inside the control volume. V_b is calculated when the partitioning of the boxes between control volumes is made. A scaling factor, s, is defined as the square root of the ratio between V_b and the volume of the combined box,

$$s = \frac{V_b}{R_x R_y} \tag{8}$$

For a uniform tracer concentration, $V_b = C_m$ and s is calculated using C_m to save CPU time.

The dimensions of the box are then adjusted as

$$R_{x_{new}} = R_x \sqrt{s}, \qquad R_{y_{new}} = R_y \sqrt{s} \tag{9}$$

If the adjusted dimensions of the box are greater than the dimensions of the containing control volume, the adjusted dimensions are set equal to those of the control volume. To conserve the tracer volume, the excess volume is transferred to the neighboring control volumes and the combined boxes of these control volumes are corrected accordingly.

4. TREATMENT OF STAGNATION POINTS

In flow fields with symmetry lines leading to stagnation points, SMM often leads to very high concentrations of tracer at the stagnation points, because the tracer boxes are assumed rigid. Those tracer boxes that are located on a symmetry line only move along the line and accumulate inside the stagnation control volume where the nodal velocity is zero. An incompressible flow field in a 'T' channel (Figure 3(a)) illustrates this point. The discretized velocity in the vertical branch is upward and twice greater than the velocity in the horizontal branches and velocity at node A is zero. SMM assumes that tracer boxes move with the velocities of the grid nodes. As a result, the tracer boxes entering the control volume A accumulate there. This is a serious problem, especially in coupled thermochemical problems where a slightly incorrect tracer field can have a major effect on the dynamics of the system.

To correct this problem, we take into account the displacements between the faces and the center of mass of a tracer box during its advection in a given time step. In a variable velocity flow field, the faces move with their respective velocities, which could be different from the velocity of the center of mass, resulting in deformation of the box. We construct a deformed shape expected for the box at the end of the time step. Following SMM, this deformed shape is then advected rigidly with the velocity of the center of mass within that time step. In other words, the distance between a given box face and the center of mass of the box at the end of a time step is calculated beforehand and the modified box is advected as a rigid body. Because the velocity values are usually available at control volume faces, the deformation of the tracer boxes relative to their centers of mass is determined by calculating how much a control volume would 'hypothetically' deform. The volume of the tracer box is then proportionally modified so that the ratio between the box volume and the volume of the 'hypothetically' deformed control volume remains unchanged.

We illustrate the procedure by applying it to the advection of a constant tracer field in the incompressible T channel mentioned before (Figure 3). The control volumes are square boxes of width L, and the time step corresponds to the Courant number of 1. The initial tracer boxes completely occupy the control volumes everywhere and their centers of mass and dimensions coincide with the grid nodes and the control volume dimensions respectively. In the control

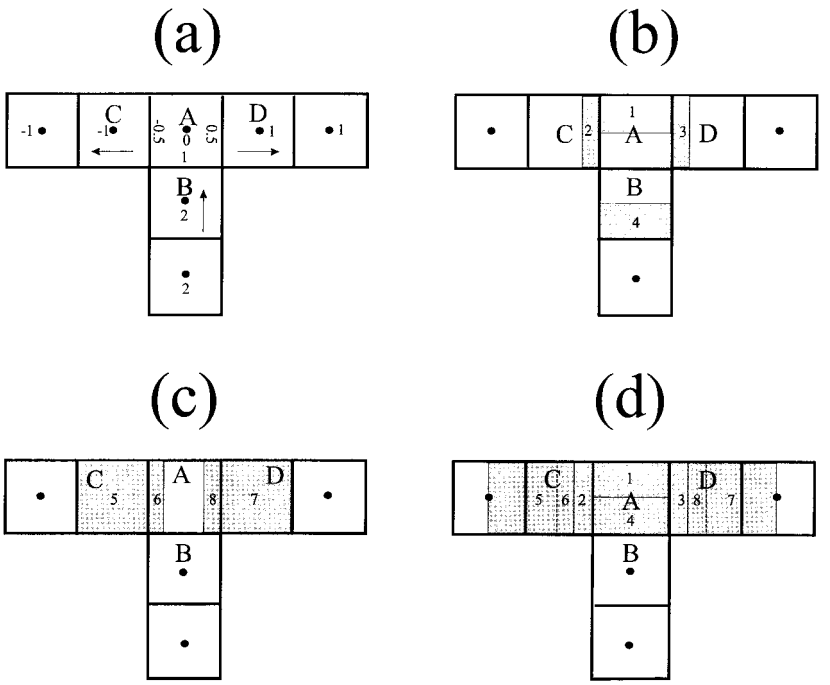

Figure 3. A T channel flow. (a) Numbers and arrows indicate nodal and interface velocities. (b) The shaded areas 1, 2 and 3 denote the redistribution of the tracer field initially in control volume A, on the basis of velocity gradients across the control volume. The shaded area 4 shows the redistributed tracer field in control volume B. (c) The shaded areas 6 and 8 denote the expanded part of tracer boxes initially in control volumes C and D respectively. The shaded areas 5 and 7 are the remaining portions of the tracer boxes, which were originally in C and D respectively. (d) The tracer distribution after being advected for one time step. At the end of the time step, the sum of the initial volumes and mass of the tracer in control volumes A, B, C and D are conserved.

volume A, the relative velocities suggest that the bottom face will displace by $0.5L$ towards node A by the end of the time step. Therefore, we shift the position of the bottom face towards node A by $0.5L$. There is no relative velocity between the top face and the nodal point, and no adjustment is required for this face. In the horizontal direction, the right-hand face of the control volume A will have a displacement of $0.25L$ to the right and the left-hand will have $0.25L$ to the left during the time step. We expand the original tracer box in the control volume A by $0.25L$ at each side to account for this displacement. The added portions are placed inside control volumes C and D (portions 2 and 3 in Figure 3(b) respectively), and treated as separate boxes whose velocities are equal to the velocity of control volume A.

In control volume B, the displacement of the top face relative to node B will be $0.5L$ toward the node at the end of the time step. We shift the position of the top face by $0.5L$ toward the node. Shaded area 4 denotes the modified tracer distribution inside B. The relative displacement between the bottom face and node B is 0 and no adjustment is required for that face.

In control volume C, the displacement of the right-hand face relative to node C at the end of the time step will be $0.25L$ toward the right, and the shaded area 6 (Figure 3(c)) denotes the shift we make. No adjustment is required for the left-hand face because its velocity is identical to that of the node. Finally, an analogous shift is made in the control volume D (shaded area 8).

Once the tracer boxes are adjusted, they are advected over the time step as rigid bodies, with the nodal velocity of their respective control volumes. Consequently, the tracer distribution in Figure 3(b) and (c) is evolved to that in Figure 3(d). Note that the total volume of the shaded areas in Figure 3(b) and (c) is equal to the initial tracer volume in the four control volumes, hence satisfying the condition of incompressibility. The tracer field is advected correctly, its volume is conserved and there is no tracer accumulation inside the stagnant control volume A.

A further shortcoming of SMM is its inability to handle a compressible flow. This difficulty arises because the rectangular distributions are treated as rigid bodies with fixed volumes, irrespective of the fact that the actual fluid material undergoes volume changes. Consequently, the tracer field will represent an inaccurate distribution of the material type that it has been assigned to. The improvement described above automatically increases or decreases the total volume of the rectangulars depending on whether the fluid is expanding or condensing. To demonstrate this point, we again use the T channel example, but with the magnitude of velocity in the horizontal branches equal to that in the vertical branch (Figure 4(a)), the fluid is now expanding. Figure 4(b) and (c) shows the adjustments before the tracer field is advected in the time step. Figure 4(d) shows the tracer distribution after being advected. The total volume of tracer has increased by one control volume in order to accommodate the expansion of the fluid medium.

5. EXAMPLES

In this section we present examples that compare the accuracy of the proposed ISMM compared with those of SMM and the Eulerian based monotonic second order upwind (MSOU) technique of Sweby [10]. Tamamidis and Assanis [11] compared the performance of MSOU with other high-order accuracy schemes, with and without flux limiters, and concluded that MSOU is one of the most accurate schemes in problems involving advection of sharp discontinuities and is nearly second-order accurate. In the MSOU method adopted here, a fourth-order Runge–Kutta method is used for discretization of the time derivative term in Equation (1). In all examples, a uniform grid of 101×101 nodes on a computational domain of $0 \leq x \leq 1$ and $0 \leq y \leq 1$ and a maximum Courant number of 0.5 is used.

5.1. Example 1: the revolving slotted cylinder

The first example is designed to compare the performance of ISMM with that of MSOU and SMM in eliminating false diffusion and enhancement. The evolution of the shape of a revolving slotted cylinder tracer field (Figure 5(a)) is studied. We choose the slotted cylinder distribution because of its sharp discontinuities and small regions of smoothness [12]. The cylinder has a radius $R_c = 15h$, where $h = 0.01$ is the uniform grid spacing, and a height of

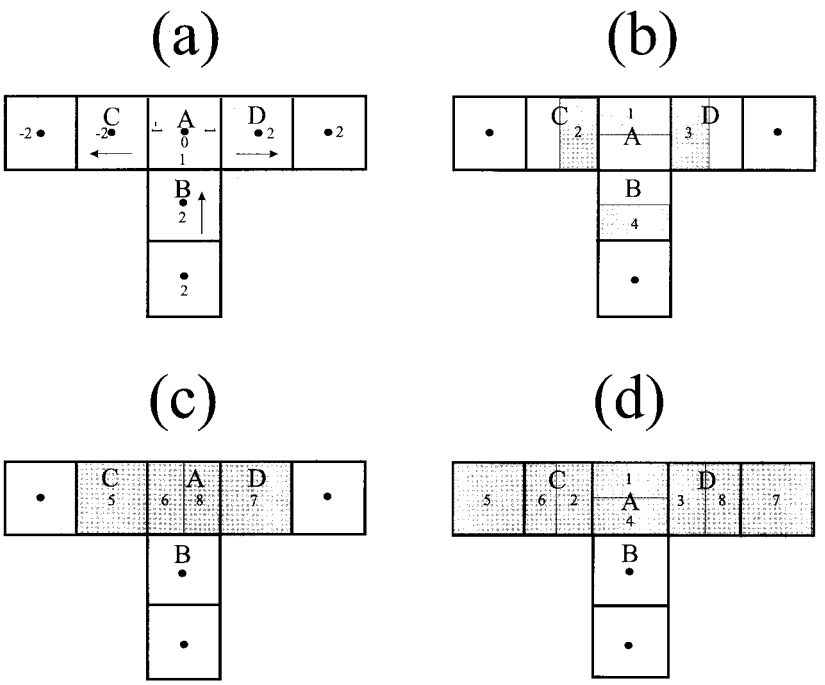

Figure 4. Compressible flow in a T channel. (a) The fluid velocity field. (b) Redistribution of the tracer box in A (shaded areas 1, 2 and 3) and B (shaded area 4) based on velocity gradients. (c) Redistribution of the tracer box in C (areas 5 and 6) and D (areas 7 and 8). (d) The tracer field after advection. The sum of the volumes of the initial tracer boxes has increased to accommodate the expansion.

$H_c = 1$. The slot has a width of $6h$ and a depth of $22h$. The angular velocity of the cylinder is $180° \text{ s}^{-1}$.

Figure 5 shows the time evolution of the shape of the cylinder calculated by MSOU, SMM and ISMM. After ten revolutions, MSOU (Figure 5(b)–(d)) still preserves the initial height of the cylinder, but the slot is gradually filled and the sharpness of the edges of the cylinder is degraded. The results of SMM (Figure 5(e)–(g)) show that after ten revolutions a significant amount of false diffusion and enhancement occurs and the slot is substantially widened. In the ISMM model (Figure 5(h)–(j)), the structure of the slot is distorted to some extent but the sharp boundaries of the cylinder are resolved over a maximum of two grid nodes.

For a quantitative comparison, the value of $\eta = \int C^2 \, dv / \int C_0^2 \, dv$, the maximum value of the tracer field (C_{max}) and an L_1 error norm are calculated and listed in Table I. C and C_0 are concentration at a given time and initial concentration respectively. L_1 is defined as

$$L_1 = \frac{1}{K} \sum_K |C - C_0| \tag{10}$$

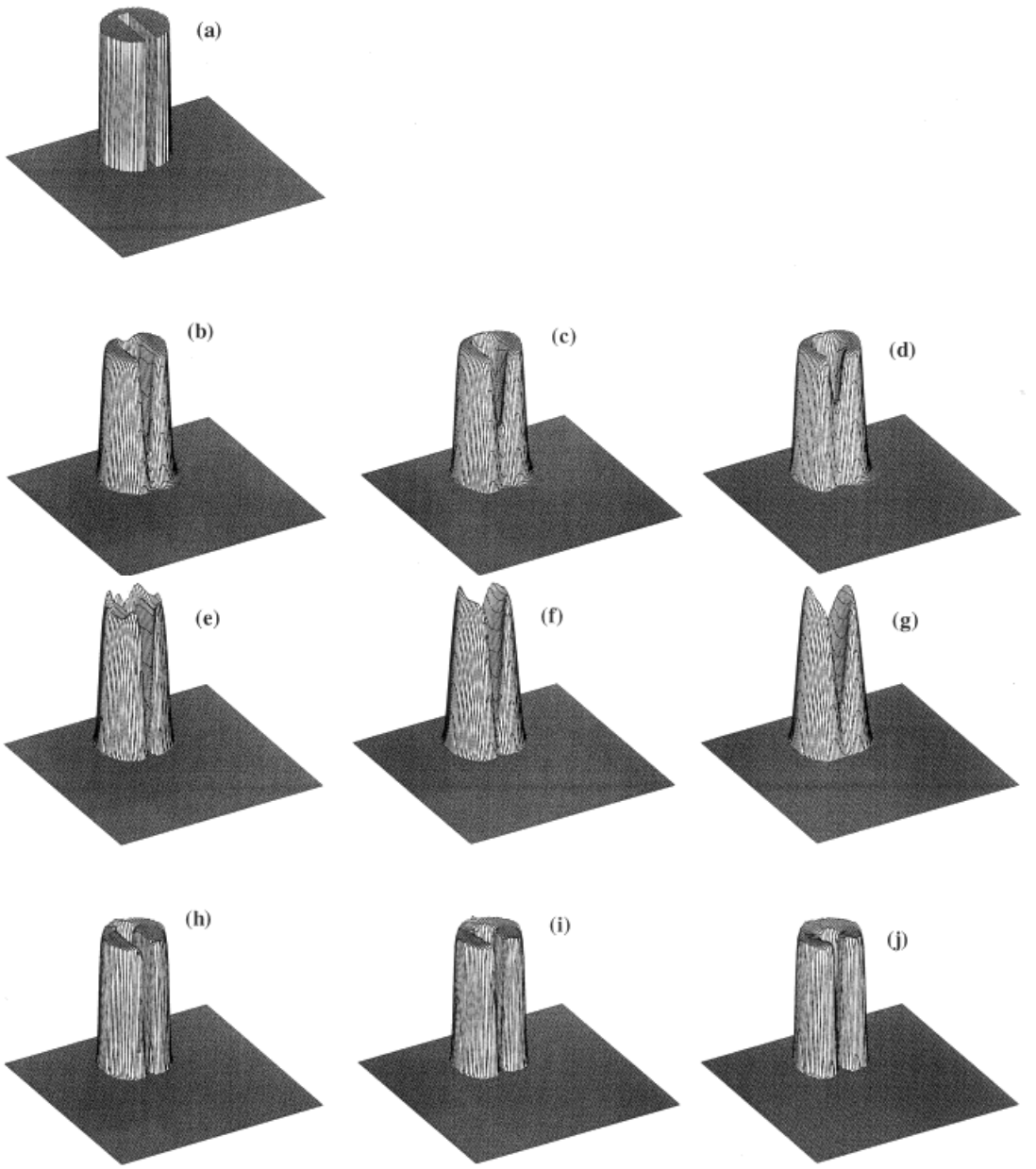

Figure 5. Deformation of a slotted cylinder. (a) The initial cylinder; shape of the cylinder obtained by MSOU after (b) one, (c) five and (d) ten revolutions; by SMM after (e) one, (f) five and (g) ten revolutions; and by ISMM after (h) one, (i) five and (j) ten revolutions.

Table I. Revolving slotted cylinder.

Number of revolutions	MSOU			SMM			ISMM		
	η	$C_{\max}$	L_1	η	$C_{\max}$	L_1	η	$C_{\max}$	L_1
1	0.83	1.0	1.4×10^{-2}	0.89	1.14	1.3×10^{-2}	0.96	1.03	4.2×10^{-3}
2	0.83	1.0	1.6×10^{-2}	0.87	1.16	1.6×10^{-2}	0.95	1.04	5.1×10^{-3}
3	0.83	1.0	1.6×10^{-2}	0.86	1.18	1.8×10^{-2}	0.96	1.03	6.0×10^{-3}
4	0.83	1.0	1.7×10^{-2}	0.84	1.19	1.9×10^{-2}	0.96	1.04	6.8×10^{-3}
5	0.83	1.0	1.7×10^{-2}	0.83	1.19	2.0×10^{-2}	0.96	1.04	7.6×10^{-3}
6	0.83	1.0	1.8×10^{-2}	0.83	1.20	2.1×10^{-2}	0.95	1.04	8.4×10^{-3}
7	0.83	1.0	1.8×10^{-2}	0.82	1.21	2.2×10^{-2}	0.95	1.04	9.1×10^{-3}
8	0.83	1.0	1.9×10^{-2}	0.81	1.22	2.3×10^{-2}	0.96	1.04	9.8×10^{-3}
9	0.83	1.0	1.9×10^{-2}	0.81	1.22	2.3×10^{-2}	0.96	1.04	1.0×10^{-2}
10	0.83	1.0	2.0×10^{-2}	0.80	1.22	2.4×10^{-2}	0.96	1.04	1.1×10^{-2}

where K is the total number of grid points. A comparison of these figures shows that for MSOU and ISMM, the value of η remains constant with the increase of integration time, suggesting that the amount of false diffusion does not change in time for these two methods. Also, MSOU and ISMM preserve the initial height of the cylinder. In contrast, SMM gives the largest diffusion and the amount of diffusion increases as the number of revolutions increases. ISMM has the best performance because after ten revolutions, L_1 of ISMM (1.1×10^{-2}) is still better than those of MSOU (1.4×10^{-2}) and SMM (1.3×10^{-2}) and its η is very close to unity.

5.2. Example 2: Smolarkiewicz deformational flow

The second example examines the performance of ISMM for the stagnation point problem, by considering the advection of a conic tracer distribution in an incompressible steady state Smolarkiewicz deformational flow field [13]. The x and y components of the velocity field are defined by

$$V_x = -\sin(4\pi x)\sin(4\pi y), \qquad V_y = -\cos(4\pi x)\cos(4\pi y) \tag{11}$$

specifying symmetrical counter-rotating vortices (Figure 6(a)) with symmetry lines in both directions and with stagnation points. The initial tracer field is a cone of radius 0.15 and height 1.0, located at the center. Figure 6(b) and (c) shows the deformed cone determined by SMM at times $t = 0.314$ s and $t = 0.628$ s respectively. A considerable amount of tracer material accumulates at the stagnation point at the top of the middle counter-rotating cells. The concentration of the tracer at point A is enhanced by a factor of 12, making the solution physically unacceptable. Figure 6(d) and (e) shows the results at the same times for ISMM. The tracer mass does not accumulate at the stagnation point, rather circulates more freely inside the convecting cells, as it is evident from the greater continuity and extension of the contour lines compared to those in the SMM plots. The maximum tracer concentration in Figure 6(d) and (e) is 1.

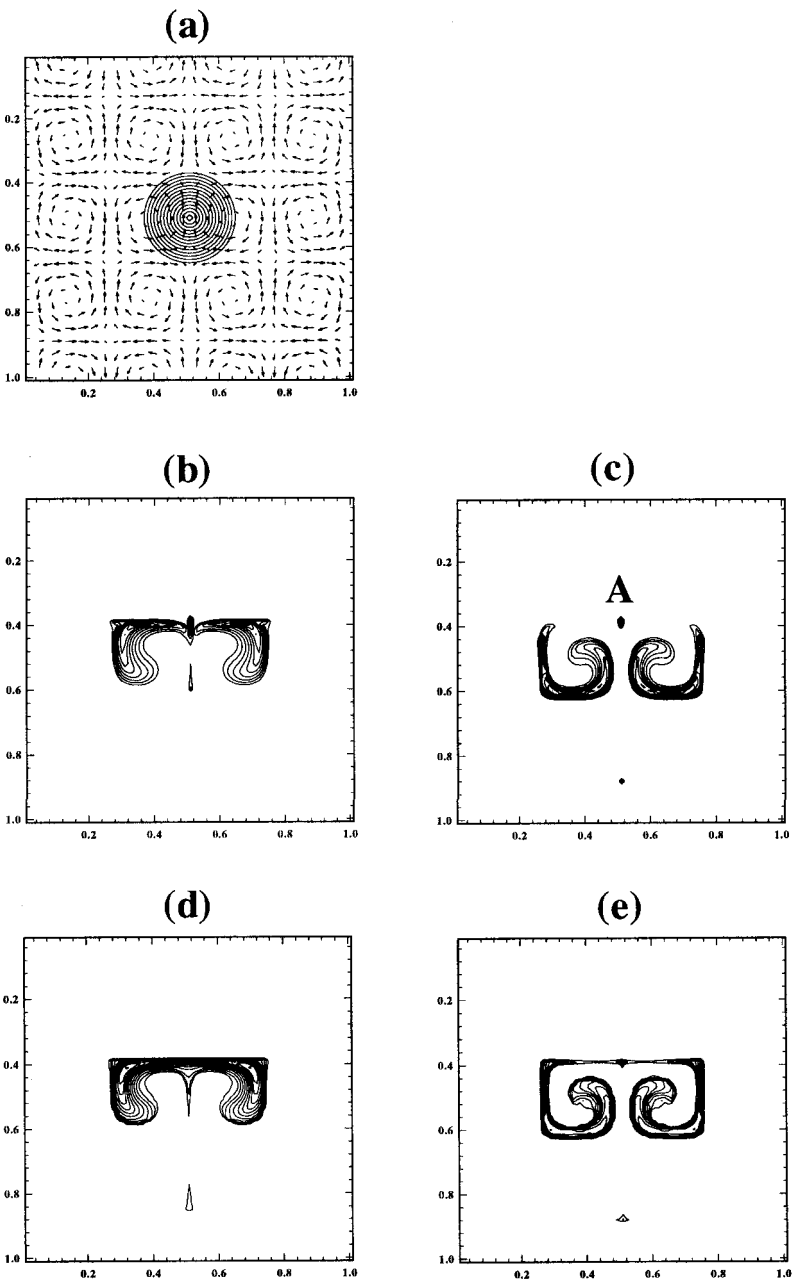

Figure 6. (a) Velocity field for Smolarkiewicz flow and the initial tracer field. The tracer field calculated by SMM at time (b) $t = 0.314$ s and (c) $t = 0.628$ s; and by ISMM at (d) $t = 0.314$ s and (e) $t = 0.628$ s.

5.3. Example 3: the twisting–untwisting experiment

In the third example, we study the advection of an initially flat layer extending from left to right (Figure 7(a)), in an incompressible flow field that alternatively rotates for 1.57 s in opposite directions, called hereafter the twisting–untwisting experiment. The velocity field is given by

$$V_x = \cos(\pi(x-0.5))\sin(\pi(y-0.5)),$$

$$V_y = -\sin(\pi(x-0.5))\cos(\pi(y-0.5)) \tag{12}$$

The sign of the velocity components changes during the untwisting part of the experiment. The initial tracer field is a layer of width 0.2 with a uniform concentration of unity. We compare the results from ISMM with those of SMM and MSOU. Figure 7 shows the tracer field at times $t = 1.57$ s and $t = 3.14$ s produced by one twist and then untwist respectively. In SMM and ISMM, the local maxima occur at the two ends of the deforming body where stretching and deformation is severe. The MSOU has the maximum false diffusion near the boundaries. In the SMM model (Figure 7(e)), the tracer field increases from 1 to a maximum of 1.8, whereas in ISMM (Figure 7(g)), the maximum value of the tracer is 1.03, which is very close to the initial value. Comparison of Figure 7(c), (e) and (g) clearly demonstrates that ISMM has a superior performance over MSOU and SMM in preserving the initial tracer field.

Figure 8 shows the profiles of the tracer field along the line $x = 0.04$ for the three methods after 0, 6, 12 and 18 twists and untwists. The MSOU solution suffers from a serious false diffusion, which increases as time passes. The numerical error for SMM is modest, but the shape-preserving quality of the method has noticeably diminished. ISMM produces the best results with a minimal false diffusion and maximum shape-preserving quality.

5.4. Example 4: compressible flow

Our final example shows how ISMM handles the problem of the transport of a color function in a compressible flow field. An initially square box of tracer field is advected in a flow field defined by

$$V_x = \cos(2\pi(x))\sin(\pi(y-0.5)),$$

$$V_y = -\sin(2\pi(x))\cos(\pi(y-0.5)) \tag{13}$$

The flow field and the regions of compression and expansion are shown in Figure 9(a). The tracer field has a width of 0.15 and is placed in the top expansional region. Figure 9(c) and (d) shows the tracer field produced by MSOU at times $t = 1.57$ and 6.28 s respectively, and Figure 9(e) and (f) shows those for ISMM. The tracer fields of ISMM are considerably less diffused than those of MSOU. Figure 9(b) shows the time evolution of the total volume of the tracer upon entering regions of expansion and compression. As time passes, the total volume reaches a statistically steady state value in the ISMM solution, which is less than the initial value. This is because the tracer field was initially in the expansional region, but later spreads over both

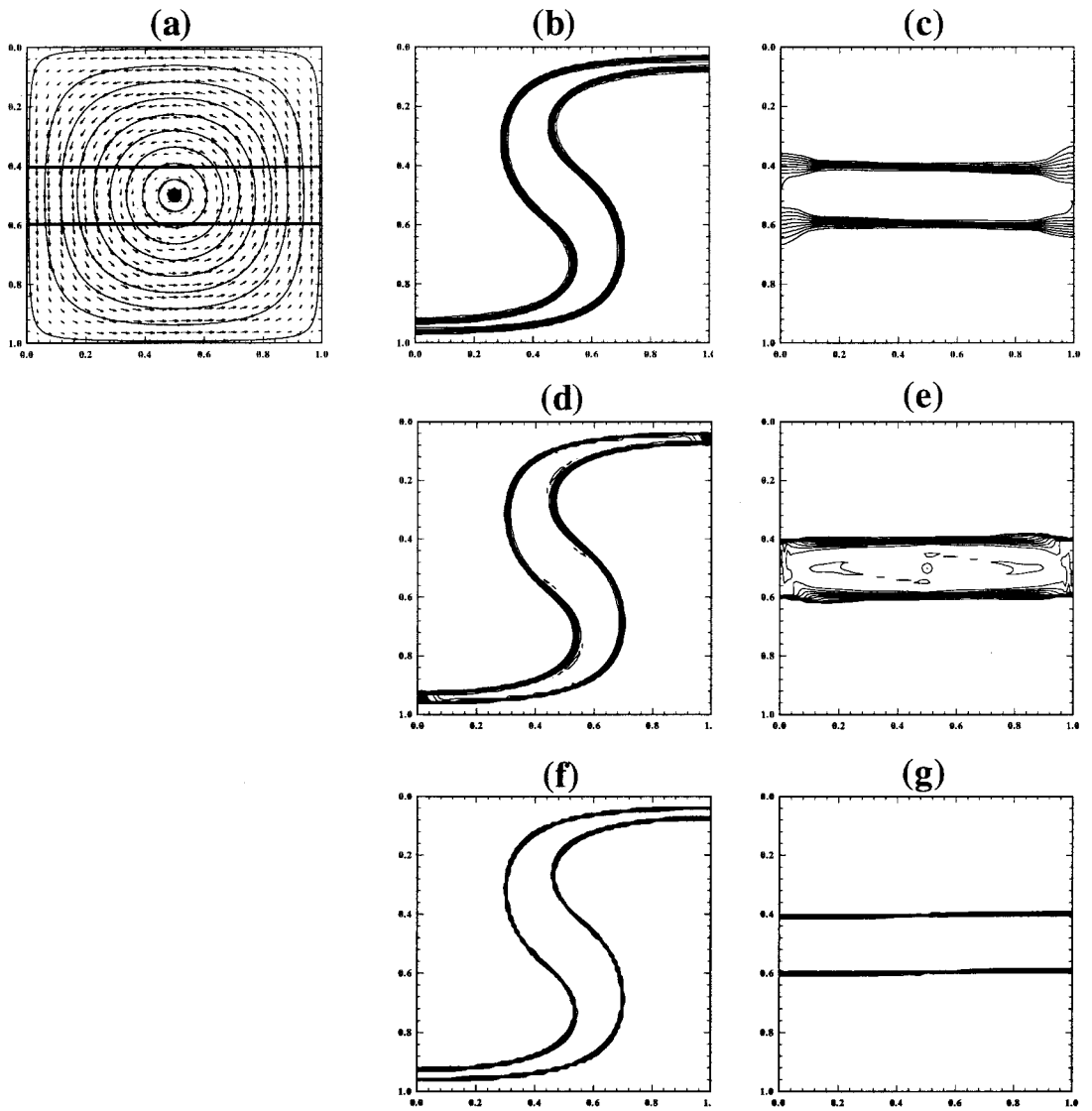

Figure 7. (a) The velocity field and the initial tracer distribution for the twisting–untwisting experiment. After 1.57 s of counterclockwise rotation the flow field is reversed. The tracer field calculated by MSOU at time (b) $t = 1.57$ s and (c) $t = 3.14$ s; by SMM at (d) $t = 1.57$ s and (e) $t = 3.14$ s; and by ISMM at (f) $t = 1.57$ s and (g) $t = 3.14$ s.

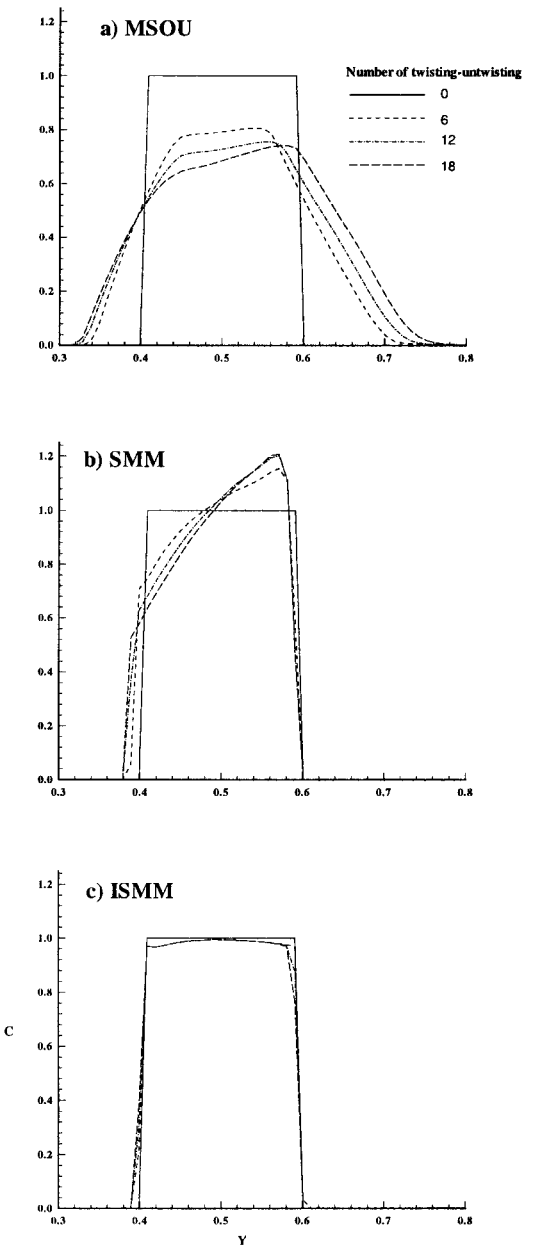

Figure 8. Profiles of tracer field along the line $x = 0.04$ in the twisting–untwisting experiment. The profiles show tracer concentration after 0, 6, 12, and 18 flow reversals for (a) MSOU, (b) SMM and (c) ISMM.

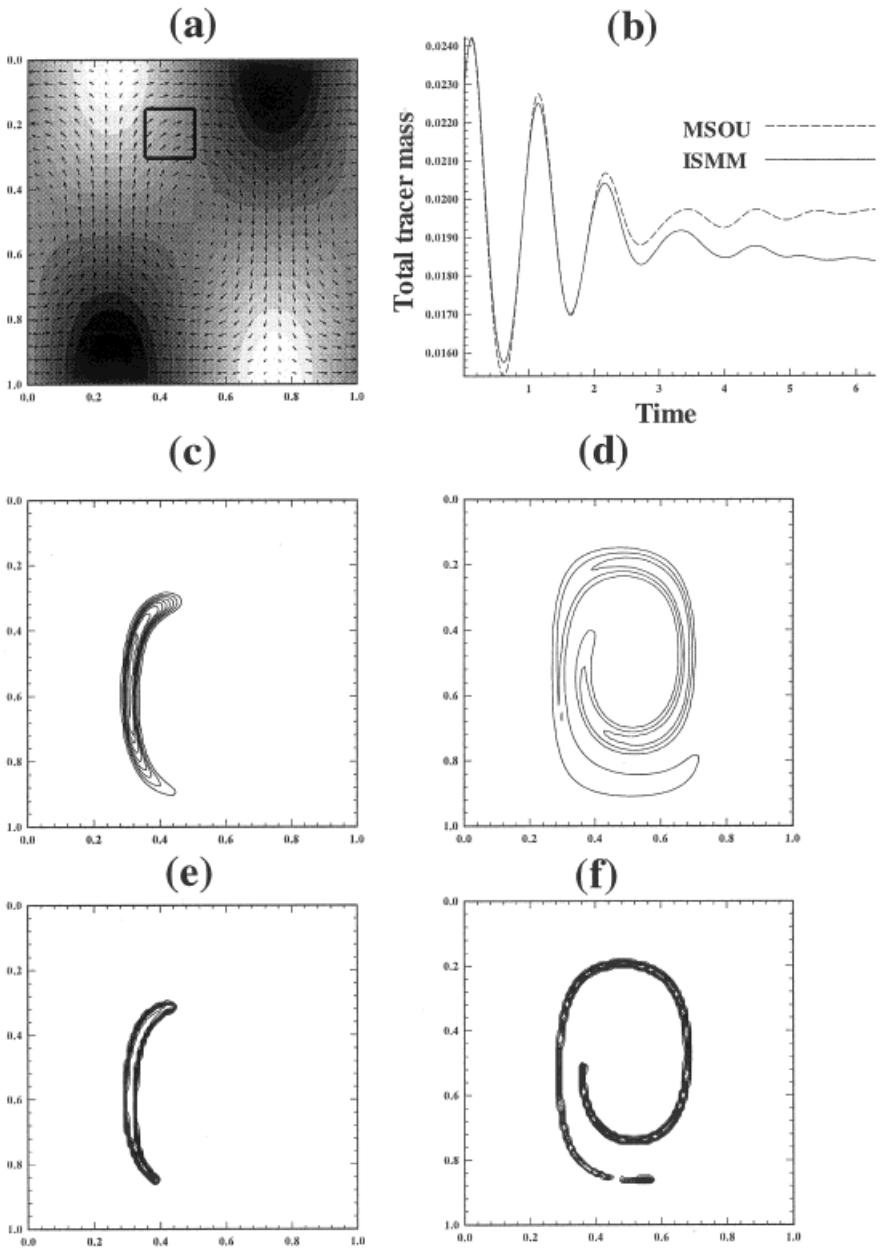

Figure 9. (a) Compressible velocity field with compressional (dark) and expansional (light) regions. The square box represents the initial tracer field. (b) Time evolution for the total tracer volume for ISMM and MSOU. The tracer field calculated by MSOU at time (c) $t = 1.57$ s and (d) $t = 6.26$ s; and by ISMM at time (e) $t = 1.57$ s and (f) $t = 6.26$ s.

the compressional and expansional regions. However, the false diffusion in MSOU results in an additional tracer volume, and the final tracer volume in MSOU approaches to a higher value than ISMM.

6. COMPUTATIONAL EFFICIENCY

In this section the computational efficiency of ISMM is compared with those of SMM and MSOU, by a spatial grid-refinement of the slotted cylinder and twisting–untwisting experiments. Following Leonard *et al.* [14], the relative cost and accuracy of each method are shown in a log–log plot of the mean square error (L_2) versus the CPU time. L_2 is defined as

$$L_2 = \frac{1}{K} \sum_{K} (C - C_0)^2 \tag{14}$$

Grid resolutions of 51×51, 101×101, 151×151 and 201×201 nodes are used. An additional experiment with a grid of 301×301 nodes is done for SMM and MSOU.

Figure 10(a) compares the computational efficiency of the three methods for the slotted cylinder. The cylinder completes one revolution in all experiments. For all resolutions, ISMM has the least amount of error. It is also faster than MSOU at low resolutions but becomes slower at higher resolutions. To obtain an error value of 1.33×10^{-3}, ISMM takes only 34.51 s on a grid of 101×101 nodes, while MSOU and SMM require about 16 min on a grid of 301×301 nodes, about 27 times more expensive than ISMM.

In Figure 10(b) the results for the twisting–untwisting experiment are displayed. Again, for a given resolution the value of error for ISMM is at least an order of magnitude less than that of both SMM and MSOU. For example, using a very fine grid of 401×401 nodes, MSOU gives an error that is four times higher than that obtained by ISMM on a grid of 51×51 nodes.

A comparison of Figure 10(a) and (b) reveals the inefficiency of SMM and MSOU compared with ISMM in the deformational flow. While in the slotted cylinder case SMM and MSOU are able to achieve the level of error of ISMM with higher resolutions and larger CPU times, in the twisting–untwisting experiment, ISMM is superior to the other methods for all resolutions.

7. CONCLUSIONS

Our primary goal was to extend the attractive features of the second moment method (SMM) to the study of strongly rotational and\or deformational flow fields. We presented two improvements to SMM in order to suppress the false diffusion\enhancement associated with the non-translational flow fields, and the mass accumulation in the stagnation points. It was shown that diffusion and\or enhancement are produced because SMM does not conserve volume. In the first improvement, the dimensions of a combined box were adjusted to conserve volume. In the second improvement, the assumption of a rigid tracer box was partially relaxed

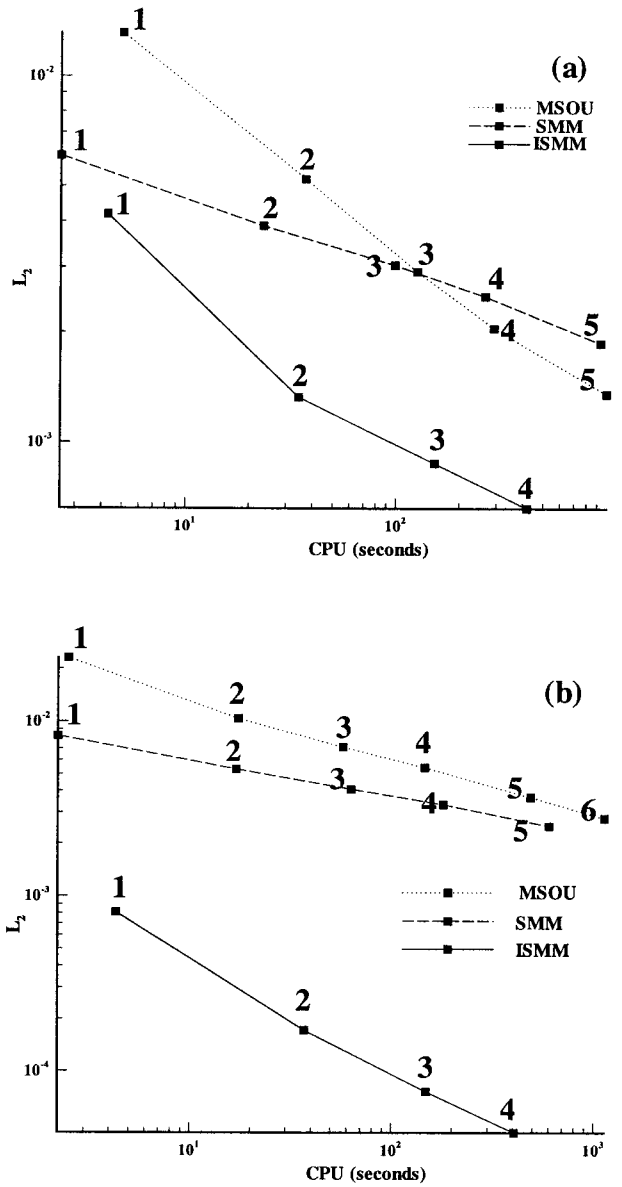

Figure 10. Computational efficiency diagrams for MSOU, SMM and ISMM with grid resolutions of (1) 51×51, (2) 101×101, (3) 151×151, (4) 201×201, (5) 301×301 and (6) 401×401 nodes. (a) Results for the slotted cylinder test and (b) for the twisting–untwisting test.

by considering normal gradients of velocity components across a given control volume. This improvement not only resolved the problem of stagnation points, but also enabled ISMM to solve a tracer field in a compressible fluid flow.

Examples showing solid body rotation, flows with stagnation points, and strong deformational flow fields were presented to illustrate the effectiveness of our improvements. It was shown that ISMM has a high quality of shape-preserving in rotational flow fields. For a given accuracy, it is far more efficient than SMM and MSOU. The ISMM technique presented here is valid for Courant numbers as high as 1 and for equal grid spacings in each direction. It requires modifications to apply for a non-uniform grid spacing. Also, the technique is more storage demanding than the Eulerian and semi-Lagrangian methods. This shortcoming is certainly overwhelmed by its advantages.

ACKNOWLEDGMENTS

This research was supported by the Natural Sciences and Engineering Research Council (NSERC) of Canada to JAH. AG and FS were partially supported by a scholarship from the Ministry of Culture and Higher Education of Iran. The authors would like to thank M. Afshar for his comments on a preliminary version of the paper, and M. Nassiri for providing the SMM Fortran code and his valuable suggestions.

REFERENCES

1. Egan BA, Mahoney JR. Numerical modeling of advection and diffusion of urban area source pollutant. *Journal of Applied Meteorology* 1972; **11**: 312–322.
2. Yeh D, Yeh G-T. Computer evaluation of high order numerical schemes to solve advective transport problems. *Computers and Fluids* 1995; **8**: 919–929.
3. Rudman M. Volume-tracking methods for interfacial flow calculations. *International Journal for Numerical Methods in Fluids* 1997; **24**: 671–691.
4. Staniforth A, Cote J. Semi-Lagrangian integration schemes for atmospheric models—a review. *Monthly Weather Review* 1991; **113**: 1050–1065.
5. Pepper DW, Baker AJ. A higher-order accurate numerical algorithm for three-dimensional transport prediction. *Computers and Fluids* 1980; **8**: 371–390.
6. Nassiri M, Babarutsi S. Computation of dye concentration in shallow recirculating flow. *Journal of Hydraulic Engineering* 1997; **123**: 793–805.
7. Tempertone C, Staniforth A. An efficient two time-level semi-Lagrangian semi-implicit integration schemes. *Quarterly Journal of the Royal Meteorological Society* 1987; **113**: 1025–1039.
8. Carmichael GR, Kitada T, Peters LK. Application of a Galerkin finite element method to atmospheric transport problems. *Computers and Fluids* 1980; **8**: 155–176.
9. Prather MJ. Numerical advection by conservation of second-order moments. *Journal of Geophysical Research* 1986; **91**: 6671–6681.
10. Sweby PK. High resolution schemes using flux limiters for hyperbolic conservation laws. *SIAM Journal of Numerical Analysis* 1984; **21**: 995–1001.
11. Tamamidis P, Assanis DN. Evaluation of various high-order-accuracy schemes with and without flux limiters. *International Journal for Numerical Methods in Fluids* 1993; **16**: 931–948.
12. Bermejo R, Staniforth A. The conversion of semi-Lagrangian advection schemes to quasi-monotone schemes. *Monthly Weather Review* 1992; **120**: 2622–2632.
13. Smolarkiewicz PK. The multi-dimensional Crowley advection scheme. *Monthly Weather Review* 1982; **110**: 1968–1983.
14. Leonard BP, Lock AP, MacVean MK. Conservative explicit unrestricted-time step multidimensional constancy-preserving advection schemes. *Monthly Weather Review* 1996; **124**: 2588–2606.

